

RIS-Enabled Passive Radar towards Target Localization

Ahmad Bazzi and Marwa Chafii

Abstract—In this paper, we study a communication-centric integrated sensing and communication (ISAC) approach, where an access point (AP) communicates with users, while a passive radar (PR) is present in the environment. We investigate the deployment of a reconfigurable intelligent surface (RIS) to enable the PR to localize a target. We derive an optimization problem for updating the phase shifters of the RIS per epoch. Due to the limited information at the PR, such as unknown payload information and unknown number of targets in the scene, we propose two methods capable of performing joint angle of arrival estimation and detection of the targets. We demonstrate the superior performance of the methods onto the proposed setting through numerical simulations, in comparison to a no-RIS baseline scheme.

Index Terms—Reconfigurable Intelligent Surfaces, Integrated Sensing and Communications, RIS, ISAC, 6G

I. INTRODUCTION

Research has begun to piece together a speculative vision of 6G by studying potential future services and applications, identifying market demands, and finding disruptive technologies [1]. A vast range of services must be supported by 6G, including blockchain, haptic telemedicine, VR/AR remote services, holographic teleportation, and huge eXtended reality (XR) capabilities. There is no doubt that 6G has advantages beyond connectivity. It will combine new functions like sensing and computing, opening up new services and employing better environmental data for artificial intelligence and machine learning. However, as [2] emphasizes, such bandwidth-hungry applications need for a $10^3 \times$ increase in capacity. Furthermore, it is anticipated that by 2030, mobile data use per mobile broadband subscriber would increase by a factor of 50, from 5.3GB in 2020 to 257GB in 2030. Nevertheless, there are several enabling technologies (such as sub-6 GHz and mmWave frequencies) and reconfigurable intelligent surface (RIS).

By ingeniously reconfiguring the wireless propagation environment, reconfigurable intelligent surfaces (RISs) have drawn a lot of attention for their potential to increase the capacity and coverage of wireless sensor networks. A RIS [3] is composed of an array of reflecting elements capable of reconfiguring incident signals, thanks to its two-dimensional material structure with programmable macroscopic physical characteristics. Since the RIS can reconfigure the electromagnetic (EM) incident wave, the wireless channel between

different nodes of the wireless network could be altered. In fact, RIS's relatively low energy consumption is one of its most appealing features because it allows for the amplification and transmission of incoming signals without the use of a power amplifier. However, because of the inexpensive cost of RIS, it may be unusually large and sprawl the entire wall of a building [4]. Instead, phase shifts applied by each reflecting element are properly designed in order to combine each reflected signal in a useful manner. In the literature, they are also referred to as large intelligent surface/antennas (LISA) [5], [6] or intelligent reflecting surfaces (IRSs) [7], [8]. Recently, RISs have been used to aid many profound applications in wireless communications, such as beamforming [9], [10], security [11], [12], orthogonal frequency-division multiplexing (OFDM) [13], [14], millimeter-wave channel estimation [15]–[18] just to name a few. There is a handful of significant advantages that could be leveraged from RIS deployment [19] in various wireless communication scenarios, such as their capability of improving the spectral and energy efficiency [20], [21], their ease of deployment and environment friendliness, compatibility with already existing standards [22], and secure wireless communications [23]. For more advantages in terms of security, energy efficiency and coverage, the interested reader is referred to [24].

Within the last 80 years, passive radar, which indicates the localization of a target by radar data without the use of own controlled emissions, had been thoroughly investigated [25]–[28]. It is highlighted in [29], that RIS is foreseen to be a key enabler for advanced localization and sensing by passive radar (PR). The deployment of passive radars possess exceptional advantages, due to their low cost [30] in terms of procurement, operation and maintenance, as well as its ability in covert operation. In PR, it is crucial to locate targets with minimal information. Indeed, the passive radar, unlike traditional radar, is protocol-agnostic. That is, the PR has no knowledge about transmit waveform information. On the other hand, PR sometimes fail to perform target localization due to lack of aid from active components.

A challenging, yet interesting, feature of 6G is integrated sensing and communications (ISAC), where the designed waveforms convey communication, as well as sensing information [1]. This allows for shared spectrum, power efficiency, in addition to hardware efficiency. ISAC can be split into three broad categories, where the first aims at a *joint design*, offering trade-offs between sensing and communications. For example, the work in [31] derives beamforming matrices for ISAC systems, under practical assumptions, such as imperfect channel state information, while [32] considers a joint design for variable length time snapshots. Another category

Ahmad Bazzi is with the Engineering Division, New York University (NYU) Abu Dhabi, 129188, UAE (email: ahmad.bazzi@nyu.edu).

Marwa Chafii is with Engineering Division, New York University (NYU) Abu Dhabi, 129188, UAE and NYU WIRELESS, NYU Tandon School of Engineering, Brooklyn, 11201, NY, USA (email: marwa.chafii@nyu.edu).

Manuscript received xxx

is *radar-centric* ISAC, where the main goal is to embed communication information onto a radar waveform, such as a chirp [33]. The last category is *communication-centric* ISAC, where one simply performs sensing using a known communication waveform, such as OFDM. The priority in this case is communications, and sensing comes as an additional feature. This is of advantage in scenarios where the communication infrastructure is established and obeys a certain protocol (ex. 802.11be/ax/ac). In this paper, we focus on a communication-centric ISAC approach, where the AP communicates with communication users and a PR is deployed to localize the targets, with the aid of RIS. An optimization framework is given to adjust the phase shifts at the RIS, and two algorithms are presented that allow simultaneous location estimation and detection of targets.

A. Existing work

Channel estimation may be required between base station (BS) and user equipment (UE) in order to design the reflective matrix, i.e the phase shifters at the RIS. For example, to design the RIS phase shifts, the approach in [34] adopts deep learning (DL) and compressed sensing (CS) techniques. This paper does not require channel estimation for target localization. [35] proposes an adaptive RIS phase shifter based on hierarchical codebooks with feedback from the UE. Even though the methodology followed in [35] performs localization, the fundamental difference lies in the scenario itself. In particular, the approach does not make use of PR and it does not leverage the multi-path bounces off the targets to perform localization. Likewise, the work in [36] also performs localization with the help of an RIS situated in the scene, but in the absence of PR. Furthermore, even though the paper in [37] presents an RIS-assisted approach for localization, the model does not comprise of reflections resulting from targets to be localized. In particular, the received signal in [37] is the direct path and the reflection resulting from the RIS. In contrast to our proposed model, where the PR performs spatial beamforming towards the RIS and focuses on the reflections bouncing off the targets towards the RIS, which in turn mirrors these bounces towards the PR. Meanwhile, the authors in [38] aim at optimizing the RIS phase shift coefficients to maximize the differences of received signal strength (RSS) values as the location changes. A similar approach utilizing RSS information appears in [39]. As opposed to [38], [39], we consider the contributions that bounce towards the RIS, then reflected towards the PR. In addition, our work does not utilize the RSS to perform target localization, as it relies on the angle of arrival (AoA) information of the different reflections.

B. Contributions and Insights

This work focuses on deploying a PR and an RIS in an existing communication scenario. The RIS would then aid the PR to perform target localization without any knowledge of the standard used. Therefore, no assumption on the transmit signal structure is required to perform target localization.

To that purpose, we have summarized our contributions below.

- **A new architecture towards target localization.** This work describes a new RIS-aided setting dedicated for target localization, which is well-suited for communication-centric ISAC systems. More specifically, a PR and an RIS are considered, where the RIS "mirrors" the reflections resulting from targets in the scene towards the PR.
- **RIS matrix optimization.** Upon "mirroring" back the reflections towards the PR, the RIS configures suitable phase shifters that could properly reflect the reflections caused only by the targets to localize.
- **Localization without knowledge of number of targets.** The PR being unaware of the dynamics of the environment, we believe that joint estimation and detection of the targets is an important task that should be carried out at the PR, with minor information about the signaling being used. Motivated by this task, we propose two methods for target localization without the need to resort to techniques that require source number enumeration, such as Akaike's information criterion (AIC) [40] and minimum description length (MDL) [41]. The proposed methods are based on normalized least mean squares (NLMS) filtering. Therefore, the proposed methods perform joint estimation and detection of targets.

Furthermore, we unveil some important insights, i.e.

- A 20 dB gain in terms of required signal-to-noise ratio (SNR) to attain an mean squared error (MSE) of 0.2 is achieved when utilizing the RIS aided target localization approach, with 16 reflective elements.
- Since the proposed methods perform simultaneous detection of number of targets, we also study the probability of detection. In this respect, a 16 dB gain in terms of required SNR for a probability of detection equal to 0.9 is attained with 16 reflective elements, as compared to a no-RIS approach. A supplemental 4 dB gain is achieved, when doubling the number of reflective elements.
- With respect to successful recovery probability (SRP), we observe gains in the order of 18 dB when localizing via the proposed RIS-aided architecture.

C. Organization and Notations

The detailed structure of this paper is given as follows,

- Section II presents the system model which includes the AP, targets and an RIS in the scene. The section describes how the PR senses the reflections mirrored by the RIS and mathematically formulates the problem at hand.
- Section III demonstrates the reflection matrix optimization technique. More specifically, it formulates and solves phase shifter components per epoch, relative to the RIS.
- Section IV presents the beamforming step at PR level. In particular, the PR should look towards the RIS in order to properly acquire all the reflections caused by the K targets. This section is dedicated towards adjusting the PR's beamforming weights.
- Section V presents the two methods for target localization performed at the PR. The methods are batch and

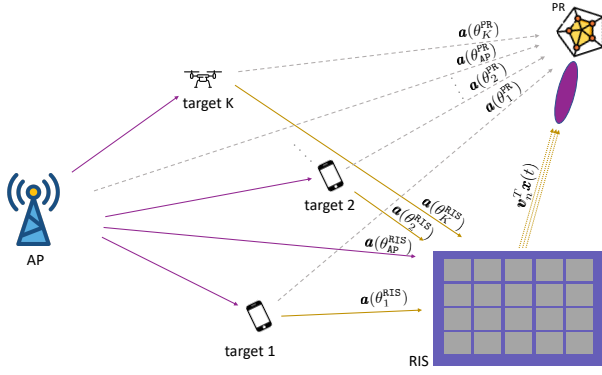


Fig. 1. The considered RIS-based multi-target system comprising of an access point simultaneously serving communication users in the downlink, where the M -element RIS reflects back the bounces off the targets towards the PR. The RIS is considered to be founded on the surrounding building's facade and the PR is in the vicinity. The transmit signal $s(t)$ propagates and bounces off the targets towards the PR, enabled by the reconfigurable behavior of the RIS. The signal $s(t)$ is any communication signal, which is also used as data to perform joint estimation and detection at the PR.

sequential versions of an NLMS filter estimate devoted for target localization through reflections.

- Section VI showcases our simulation results and the superiority of the setting, when compared to the baseline approach, i.e. when no RIS is employed. We perform target localization using both introduced methods and study the performance via different metrics, such as the MSE, SRP, and probability of detection.
- Section VII concludes the paper and provides future insights and ideas.

Notation: : Upper-case and lower-case boldface letters denote matrices and vectors, respectively. $(\cdot)^T$, $(\cdot)^*$ and $(\cdot)^H$ represent the transpose, the conjugate and the transpose-conjugate operators. The statistical expectation is denoted as $\mathbb{E}\{\cdot\}$. For any complex number $z \in \mathbb{C}$, the magnitude is denoted as $|z|$, its angle is $\angle z$. The ℓ_2 norm of a vector \mathbf{x} is denoted as $\|\mathbf{x}\|$. The matrix \mathbf{I}_N is the identity matrix of size $N \times N$. The zero-vector is $\mathbf{0}$. For matrix indexing, the $(i, j)^{th}$ entry of matrix \mathbf{A} is denoted by $\mathbf{A}_{i,j}$. The sub-matrix of \mathbf{A} ranging from rows i_1 to $i_2 > i_1$ and columns j_1 to $j_2 > j_1$ is denoted as $\mathbf{A}_{i_1:i_2, j_1:j_2}$.

II. SYSTEM MODEL

Let us assume a narrow-band system where K targets are to be localized. Note that communication users will likewise be localized as they are also regarded as targets. For simplicity, assume that the base station is equipped with a single antenna and transmits a signal $s(t)$. Note that in a communication-centric ISAC setting, the signal $s(t)$, which is meant for communications, is leveraged by the radar sub-systems as well, i.e. the PR. In the downlink, since the signal $s(t)$, intended for a specific communication user, is transmitted by a base station via an omni-directional antenna, the signal $s(t)$ is broadcasted. The signal would then hit K targets. The RIS receives the bounces off the K targets, as well as the direct path between

the AP and itself. Therefore, the received signal at the RIS reads

$$\mathbf{r}(t) = \mathbf{A}(\Theta_{1:K}^{\text{RIS}})\mathbf{s}(t) + \alpha_0 \mathbf{a}_M(\theta_{\text{AP}}^{\text{RIS}})s(t - \tau_{\text{AP}}^{\text{RIS}}), \quad (1)$$

where $\Theta_{1:K}^{\text{RIS}} = [\theta_1^{\text{RIS}} \ \theta_2^{\text{RIS}} \ \dots \ \theta_K^{\text{RIS}}]$ and θ_k^{RIS} is the angle between the k^{th} target and the RIS. Furthermore, the angle $\theta_{\text{AP}}^{\text{RIS}}$ is the angle between the AP and the RIS. The matrix $\mathbf{A}(\Theta_{1:K}^{\text{RIS}})$ is the steering matrix, which results from the contribution of each path between the targets and the RIS, namely

$$\mathbf{A}(\Theta_{1:K}^{\text{RIS}}) = [\mathbf{a}_M(\theta_1^{\text{RIS}}) \ \mathbf{a}_M(\theta_2^{\text{RIS}}) \ \dots \ \mathbf{a}_M(\theta_K^{\text{RIS}})], \quad (2)$$

where $\mathbf{a}_M(\theta) \in \mathbb{C}^{M \times 1}$ is the steering vector at the output of the M -elements of the RIS. The concatenation of all steering vectors defines the array manifold, $\mathbf{A}(\Theta_{1:K}^{\text{RIS}}) \in \mathbb{C}^{M \times K}$. It is worth noting that this paper does not assume any structure on $\mathbf{a}_M(\theta)$. The signal $\mathbf{s}(t)$ contains scaled and delayed versions of the original transmitted signal $s(t)$, and is represented as

$$\mathbf{s}(t) = \begin{bmatrix} \alpha_1 s(t - \tau_{\text{AP}}^1 - \tau_1^{\text{RIS}}) \\ \alpha_2 s(t - \tau_{\text{AP}}^2 - \tau_2^{\text{RIS}}) \\ \vdots \\ \alpha_K s(t - \tau_{\text{AP}}^K - \tau_K^{\text{RIS}}) \end{bmatrix} \in \mathbb{C}^{K \times 1}, \quad (3)$$

where τ_{AP}^k is the propagation delay between the AP and the k^{th} target, τ_k^{RIS} is the propagation delay between the k^{th} target and the RIS, and $\tau_{\text{AP}}^{\text{RIS}}$ is the propagation delay between the AP and the RIS. Furthermore, the complex coefficient α_k , for $k = 1 \dots K$, is the reflection gain, taking into account large scale fading effects, resulting from the path between the AP towards the k^{th} target then towards the RIS. Likewise, α_0 is the complex coefficient taking into account the channel gain between the AP and the RIS. Furthermore, the reflected signal from the RIS towards the PR is expressed as

$$x_n(t) = \mathbf{v}_n^T \left(\mathbf{A}(\Theta_{1:K}^{\text{RIS}})\mathbf{s}(t) + \alpha_0 \mathbf{a}_M(\theta_{\text{AP}}^{\text{RIS}})s(t - \tau_{\text{AP}}^{\text{RIS}}) \right), \quad (4)$$

where $\mathbf{v}_n \in \mathbb{C}^{M \times 1}$ is the phase shifts due to the reflecting elements of the RIS at the n^{th} epoch. We define the epoch as a period of time receiving a realization of $\mathbf{r}(t)$ defined in equation (1). The final received signal at the PR is expressed over three counterparts as follows

$$\begin{aligned} \mathbf{y}_n(t) &= \rho_{\text{RIS}}^{\text{PR}} \mathbf{a}(\theta_{\text{RIS}}^{\text{PR}})x_n(t - \tau_{\text{RIS}}^{\text{PR}}) \\ &+ \rho_{\text{AP}}^{\text{PR}} \mathbf{a}(\theta_{\text{AP}}^{\text{PR}})s(t - \tau_{\text{AP}}^{\text{PR}}) \\ &+ \sum_{k=1}^K \rho_k \mathbf{a}(\theta_k^{\text{PR}})s(t - \tau_{\text{AP}}^k - \tau_k^{\text{PR}}) + \boldsymbol{\epsilon}_n(t), \end{aligned} \quad (5)$$

where $\mathbf{y}_n(t) \in \mathbb{C}^{N_{\text{PR}} \times 1}$ is the received signal at the PR. The first term, i.e. $\rho_{\text{RIS}}^{\text{PR}} \mathbf{a}(\theta_{\text{RIS}}^{\text{PR}})x_n(t - \tau_{\text{RIS}}^{\text{PR}})$, contains all information gathered at the RIS and reflected back towards the PR. The second term, namely $\rho_{\text{AP}}^{\text{PR}} \mathbf{a}(\theta_{\text{AP}}^{\text{PR}})s(t - \tau_{\text{AP}}^{\text{PR}})$, consists of the direct LoS between the AP and the PR. The third term, that is $\sum_{k=1}^K \rho_k \mathbf{a}(\theta_k^{\text{PR}})s(t - \tau_{\text{AP}}^k - \tau_k^{\text{PR}})$, contains K target contributions that propagated from the AP towards the targets then bounced off the targets towards the PR. The propagation delay $\tau_{\text{RIS}}^{\text{PR}}$ is the delay between the RIS and the PR, $\tau_{\text{AP}}^{\text{PR}}$ is the delay between AP and the PR and τ_k^{PR} is the delay between the k^{th} target and

the PR. Moreover, the large scale fading gains ρ_k 's are defined in a similar manner as α_k 's. Furthermore, the noise term $\boldsymbol{\epsilon}_n(t)$ is additive white Gaussian background noise. Sampling at L time instances, we have

$$\begin{aligned} \mathbf{Y}_n &= [\mathbf{y}_n(1) \quad \mathbf{y}_n(2) \quad \dots \quad \mathbf{y}_n(L)] \\ &= \rho_{\text{RIS}}^{\text{PR}} \mathbf{a}(\theta_{\text{RIS}}^{\text{PR}}) \mathbf{x}_n + \rho_{\text{AP}}^{\text{PR}} \mathbf{a}(\theta_{\text{AP}}^{\text{PR}}) \mathbf{s}_{\text{AP}}^{\text{PR}} + \sum_{k=1}^K \rho_k \mathbf{a}(\theta_k^{\text{PR}}) \mathbf{s}_k^{\text{PR}} + \mathbf{E}_n, \end{aligned} \quad (6)$$

where $\mathbf{Y}_n \in \mathbb{C}^{N_{\text{PR}} \times L}$ is the sampled data matrix at the PR at the n^{th} epoch. Also,

$$\mathbf{x}_n = [x_n(t_1) \quad x_n(t_2) \quad \dots \quad x_n(t_L)], \quad (7)$$

$$\mathbf{s}_{\text{AP}}^{\text{PR}} = \begin{bmatrix} s(t_1 - \tau_{\text{AP}}^{\text{PR}}) \\ s(t_2 - \tau_{\text{AP}}^{\text{PR}}) \\ \vdots \\ s(t_L - \tau_{\text{AP}}^{\text{PR}}) \end{bmatrix}^T, \quad (8)$$

$$\mathbf{s}_k^{\text{PR}} = \begin{bmatrix} s(t_1 - \tau_{\text{AP}}^k - \tau_k^{\text{PR}}) \\ s(t_2 - \tau_{\text{AP}}^k - \tau_k^{\text{PR}}) \\ \vdots \\ s(t_L - \tau_{\text{AP}}^k - \tau_k^{\text{PR}}) \end{bmatrix}^T, \quad (9)$$

$$\mathbf{E}_n = [\boldsymbol{\epsilon}_n(t_1) \quad \boldsymbol{\epsilon}_n(t_2) \quad \dots \quad \boldsymbol{\epsilon}_n(t_L)]^T. \quad (10)$$

Collecting all samples at different epochs in one data matrix, we now have the following at the PR,

$$\mathbf{Y} = \begin{bmatrix} \mathbf{Y}_1 \\ \mathbf{Y}_2 \\ \vdots \\ \mathbf{Y}_N \end{bmatrix} \in \mathbb{C}^{N_{\text{PR}} N_{\text{epoch}} \times L}. \quad (11)$$

Now, we are ready to address our problem, i.e. *given our data matrix \mathbf{Y} , which contains information over different trajectories, time instances and passive radar sensors, our objective is to estimate the angles of arrivals of the targets that bounced off the RIS towards the PR.*

III. REFLECTION MATRIX OPTIMIZATION

The RIS reflection matrix is used for radar-centric sensing performance enhancements. Our goal is to maximize the contributions of the K targets collected at the RIS and minimize the power of all other contributions, which in this case come from the AP. At the n^{th} epoch, one possible optimization problem would be to

$$(\mathcal{P}_{\text{RIS}}) : \begin{cases} \min_{\mathbf{v}_n} & \|\mathbf{v}_n^T \mathbf{a}(\theta_{\text{AP}}^{\text{RIS}})\|^2 \\ \text{s.t.} & |\mathbf{v}_n| = 1. \end{cases} \quad (12)$$

Note that in the above, we have decided not to create specific beams towards the PR, as we can have multiple PRs in the scene. Therefore, the objective aims at minimizing the known static contribution between AP and RIS. Also, the above problem acts on an instantaneous basis, that is it optimizes the reflection coefficients of the RIS based on observations at

the n^{th} epoch only. To minimize over all epochs, we propose the following criterion,

$$(\mathcal{P}_{\text{RIS}}) : \begin{cases} \min_{\mathbf{V}} & \|\mathbf{V} \mathbf{a}(\theta_{\text{AP}}^{\text{RIS}})\|^2 \\ \text{s.t.} & |\mathbf{V}_{i,j}| = 1, \end{cases} \quad (13)$$

where $\mathbf{V} = [\mathbf{v}_1 \quad \mathbf{v}_2 \quad \dots \quad \mathbf{v}_{N_{\text{epoch}}}]^T \in \mathbb{C}^{N_{\text{epoch}} \times M}$. The above problem is obviously a non-convex optimization problem. To this end, we propose to first relax the problem as follows: 1) solve the unconstrained optimization problem then 2) adapt the solution towards a feasible one. Following this approach, the solution of the unconstrained variant of $(\mathcal{P}_{\text{RIS}})$ is

$$\bar{\mathbf{V}} = \mathcal{P}_{\mathbf{a}(\theta_{\text{AP}}^{\text{RIS}})}^\perp = \mathbf{I}_M - \frac{1}{\|\mathbf{a}(\theta_{\text{AP}}^{\text{RIS}})\|^2} \mathbf{a}(\theta_{\text{AP}}^{\text{RIS}}) \mathbf{a}^H(\theta_{\text{AP}}^{\text{RIS}}), \quad (14)$$

which constitutes a one-time computation. Next, the solution is in-feasible, since there is no guarantee that $\bar{\mathbf{V}}_{i,j}$ satisfies the constant modulus constraint.

$$\mathbf{V} = \exp \left\{ j \angle (\mathcal{P}_{\mathbf{a}(\theta_{\text{AP}}^{\text{RIS}})}^\perp \boldsymbol{\Gamma}) \right\}, \quad (15)$$

where $\boldsymbol{\Gamma} \in \mathbb{C}^{M \times N_{\text{epoch}}}$ is a random matrix drawn from a standard Gaussian distribution. Note that the solution, \mathbf{V} is independent of the signal $s(t)$, hence no signal knowledge is required at the RIS, as well as the PR.

IV. BEAMFORMING TOWARDS RIS

First, let us assume that the PR beamforms towards the RIS using the same beamforming vector \mathbf{w} over all time epochs as follows

$$\mathbf{Z} = \begin{bmatrix} \mathbf{w}^H \mathbf{Y}_1 \\ \mathbf{w}^H \mathbf{Y}_2 \\ \vdots \\ \mathbf{w}^H \mathbf{Y}_N \end{bmatrix} = [\mathbf{z}_1 \quad \dots \quad \mathbf{z}_L] \in \mathbb{C}^{N_{\text{epoch}} \times L}. \quad (16)$$

Notice that the output of the beamformer at any epoch n is given as follows

$$\begin{aligned} \mathbf{w}^H \mathbf{Y}_n &= \rho_{\text{RIS}}^{\text{PR}} \mathbf{w}^H \mathbf{a}(\theta_{\text{RIS}}^{\text{PR}}) \mathbf{x}_n \\ &+ \underbrace{\mathbf{w}^H \left(\rho_{\text{AP}}^{\text{PR}} \mathbf{a}(\theta_{\text{AP}}^{\text{PR}}) \mathbf{s}_{\text{AP}}^{\text{PR}} + \sum_{k=1}^K \rho_k \mathbf{a}(\theta_k^{\text{PR}}) \mathbf{s}_k^{\text{PR}} + \mathbf{E}_n \right)}_{\text{interference + noise}}. \end{aligned} \quad (17)$$

Aiming at maximizing the output power over all epochs, we can propose the following optimization problem

$$(\mathcal{P}_1) : \begin{cases} \max_{\mathbf{w}} & \sum_{n=1}^N \mathbf{R}_{x_n x_n} \\ \text{s.t.} & \mathbf{w}^H \mathbf{a}(\theta_{\text{RIS}}^{\text{PR}}) = 1, \end{cases} \quad (18)$$

where $\mathbf{R}_{x_n x_n}$ is the output power contribution of the useful part looking in the direction of $\theta_{\text{RIS}}^{\text{PR}}$

$$\mathbf{R}_{x_n x_n} = |\alpha_n|^2 \mathbf{w}^H \mathbf{a}(\theta_{\text{RIS}}^{\text{PR}}) \mathbf{a}^H(\theta_{\text{RIS}}^{\text{PR}}) \mathbf{w}, \quad (19)$$

where $\alpha_n = \rho_{\text{RIS}}^{\text{PR}} \sqrt{\mathbf{x}_n^T \mathbf{x}_n^*}$. The Lagrangian function associated with the above optimization problem is given as follows

$$\mathcal{L}(\mathbf{w}, \lambda) = |\alpha|^2 \mathbf{w}^H \mathbf{a}(\theta_{\text{RIS}}^{\text{PR}}) \mathbf{a}^H(\theta_{\text{RIS}}^{\text{PR}}) \mathbf{w} - \lambda (\mathbf{w}^H \mathbf{a}(\theta_{\text{RIS}}^{\text{PR}}) - 1), \quad (20)$$

where $|\alpha|^2 = \sum_{n=1}^N |\alpha_n|^2$. Deriving with respect to \mathbf{w} , we get the following expression

$$\frac{\partial}{\partial \mathbf{w}} \mathcal{L}(\mathbf{w}, \lambda) = 2|\alpha|^2 \mathbf{a}(\theta_{\text{RIS}}^{\text{PR}}) \mathbf{a}^H(\theta_{\text{RIS}}^{\text{PR}}) \mathbf{w} - \lambda \mathbf{a}(\theta_{\text{RIS}}^{\text{PR}}), \quad (21)$$

which is null at

$$\mathbf{w} = \frac{\mathbf{a}(\theta_{\text{RIS}}^{\text{PR}})}{\|\mathbf{a}(\theta_{\text{RIS}}^{\text{PR}})\|^2}, \quad (22)$$

and

$$\lambda = 2|\alpha|^2. \quad (23)$$

To this end, and after beamforming via equation (22), our model becomes

$$\mathbf{Z}_n = \mathbf{w}^H \mathbf{Y}_n = \rho_{\text{RIS}}^{\text{PR}} \mathbf{x}_n + \mathbf{i}_n + \tilde{\mathbf{e}}_n, \quad (24)$$

with

$$\mathbf{i}_n = \rho_{\text{AP}}^{\text{PR}} \beta(\theta_{\text{AP}}^{\text{PR}}) \mathbf{s}_{\text{AP}}^{\text{PR}} + \sum_{k=1}^K \rho_k \beta(\theta_k^{\text{PR}}) \mathbf{s}_k^{\text{PR}}, \quad (25)$$

where $\tilde{\mathbf{e}}_n = \mathbf{w}^H \mathbf{E}_n$ and $\beta(\theta) = \mathbf{w}^H \mathbf{a}(\theta)$ is the output of the beam pattern used with our beamforming vector to maximize the power in the direction of $\theta_{\text{RIS}}^{\text{PR}}$. With increasing number of antennas for ULAs, it is easily verified that $\beta(\theta) \xrightarrow[N_{\text{PR}} \rightarrow \infty]{} 0$ for all $\theta \neq \theta_{\text{RIS}}^{\text{PR}}$. Therefore, this means that all signal contributions that are not reflected by the RIS, $\mathbf{i}_n \xrightarrow[N_{\text{PR}} \rightarrow \infty]{} \mathbf{0}$. After beamforming at each time epoch, the collected data are stacked as

$$\mathbf{Z} = \begin{bmatrix} \mathbf{w}^H \mathbf{Y}_1 \\ \mathbf{w}^H \mathbf{Y}_2 \\ \vdots \\ \mathbf{w}^H \mathbf{Y}_{N_{\text{epoch}}} \end{bmatrix} = [\mathbf{z}_1 \quad \mathbf{z}_2 \quad \dots \quad \mathbf{z}_L], \quad (26)$$

where $\mathbf{Z} \in \mathbb{C}^{N_{\text{epoch}} \times L}$ is the beamformed data matrix at the PR over all epochs and time samples. In the next section, we describe two methods that process \mathbf{Z} in two different manners, i.e. as a batch or sequentially.

V. TARGET LOCALIZATION

Given a matrix \mathbf{Z} at the passive radar, the task is to estimate all angles within $\Theta_{1:K}^{\text{RIS}}$, which consists of all target AoA information. However, in many situations, such as dynamic environments, the number of targets, i.e. K , may be unknown. To this end, consider the output of the sum-and-delay beamformer at direction θ utilizing the steering vector $\mathbf{V}\mathbf{a}(\theta)$ at the ℓ^{th} snapshot, namely

$$p_\ell(\theta) = \mathbf{a}^H(\theta) \mathbf{V}^H \mathbf{z}_\ell. \quad (27)$$

Then, we can define the error cost function that we try to minimize at each snapshot, i.e.

$$C(\ell) = \mathbb{E}(|e(\ell)|^2), \quad (28)$$

where $e(\ell) = p_\ell(\theta) - \mathbf{a}^H \mathbf{z}_\ell$. The least-mean square aims at minimizing the above cost. First, we take the gradient with respect to \mathbf{a} to get

$$\begin{aligned} \nabla_{\mathbf{a}} C(\ell) &= 2\mathbb{E}\{\nabla_{\mathbf{a}}[e(\ell)]e^*(\ell)\} \\ &= -2\mathbb{E}\{(p_\ell(\theta) - \mathbf{a}^H \mathbf{z}_\ell)^* \mathbf{z}_\ell\}, \end{aligned} \quad (29)$$

where the last step is due to the gradient's value, $\nabla_{\mathbf{a}}[e(\ell)] = -\mathbf{z}_\ell$. Thanks to $\nabla_{\mathbf{a}} C(\ell)$, the least mean squares (LMS) filter can now focus towards the steepest ascent of $C(\ell)$ by taking a direction opposite to $\nabla_{\mathbf{a}} C(\ell)$, namely

$$\begin{aligned} \hat{\mathbf{a}}_{\ell+1}(\theta) &= \hat{\mathbf{a}}_\ell(\theta) - \frac{\mu}{2} [\nabla_{\mathbf{a}} C(\ell)]_{\mathbf{a}=\hat{\mathbf{a}}_\ell} \\ &= \hat{\mathbf{a}}_\ell(\theta) + \mu \mathbb{E}\{(p_\ell(\theta) - \hat{\mathbf{a}}_\ell^H(\theta) \mathbf{z}_\ell)^* \mathbf{z}_\ell\}, \end{aligned} \quad (30)$$

where $\frac{\mu}{2}$ is the well-known LMS adaptation constant, i.e. the step size. Now that we have an update equation for the steering vector in the θ 's look-direction, the only problem that remains is the expectation operator, which is not available at time update ℓ . Therefore, omitting it we finally have

$$\hat{\mathbf{a}}_{\ell+1}(\theta) = \hat{\mathbf{a}}_\ell(\theta) + \mu(p_\ell(\theta) - \hat{\mathbf{a}}_\ell^H(\theta) \mathbf{z}_\ell)^* \mathbf{z}_\ell. \quad (31)$$

A normalized LMS, i.e. NLMS, could also be proposed at this point to avoid sensitivities of the input norm, i.e. $\|\mathbf{z}_\ell\|$, which makes it extremely difficult to choose an adaptation constant for algorithm stability purposes [42]. To this end, the following update is proposed

$$\hat{\mathbf{a}}_{\ell+1}(\theta) = \hat{\mathbf{a}}_\ell(\theta) + \frac{\mu}{\|\mathbf{z}_\ell\|} (p_\ell(\theta) - \hat{\mathbf{a}}_\ell^H(\theta) \mathbf{z}_\ell)^* \mathbf{z}_\ell. \quad (32)$$

Since $\hat{\mathbf{a}}(\theta)$ also contains signal contributions present on direction θ , then a reasonable spectrum would be to measure the total power contained in the final estimate $\hat{\mathbf{a}}_L(\theta)$, namely

$$P(\theta) = \|\hat{\mathbf{a}}_L(\theta)\|^2. \quad (33)$$

Finally, the angles of arrival (AoAs) corresponding to the K targets are computed through a one-dimensional peak-finding search of $P(\theta)$, viz.

$$\hat{\Theta}_{1:K}^{\text{RIS}} = \arg \max_{\theta_1 \dots \theta_K} P(\theta). \quad (34)$$

A summary of an implementation of the proposed LMS filtering approach is summarized in **Algorithm 1**. One interesting feature of this batch approach is that it could be parallelized over angles to be evaluated on a grid, i.e. Θ_{grid} .

Algorithm 1 Batch NLMS filter Localization

```

INPUT  $\mathbf{Z} = [\mathbf{z}_1 \quad \dots \quad \mathbf{z}_L]$ ,  $\mu$ ,  $\Theta_{\text{grid}}$ 
while  $\theta \neq \emptyset$  do
     $\hat{\mathbf{a}}_0(\theta) \leftarrow \mathbf{0}_{N_{\text{epoch}} \times 1}$ 
     $\ell \leftarrow 0$ 
    while  $\ell < L$  do
         $p_\ell(\theta) \leftarrow \mathbf{a}^H(\theta) \mathbf{V}^H \mathbf{z}_\ell$ 
         $\hat{\mathbf{a}}_{\ell+1}(\theta) \leftarrow \hat{\mathbf{a}}_\ell(\theta) + \frac{\mu}{\|\mathbf{z}_\ell\|} (p_\ell(\theta) - \hat{\mathbf{a}}_\ell^H(\theta) \mathbf{z}_\ell)^* \mathbf{z}_\ell$ 
         $\ell \leftarrow \ell + 1$ 
    end while
     $P(\theta) = \|\hat{\mathbf{a}}_L(\theta)\|^2$ 
    Choose next  $\theta \in \Theta_{\text{grid}}$ 
end while
if  $P(\theta)$  is peak then
    Insert  $\theta$  in  $\hat{\Theta}_{1:K}^{\text{RIS}}$ 
end if

return  $\hat{\Theta}_{1:K}^{\text{RIS}}$ 
    
```

Note that for peak detection, we first normalize the entire spectrum $P(\theta)$ so that its maximum value is 1. Then, we use MATLAB's `findpeaks()` function to determine the peaks that exceed a certain threshold value, say $0 < \varphi < 1$.

Even though the implementation of **Algorithm 1** is sequential over snapshot dimensions, i.e. over the columns of \mathbf{Z} , one would have to wait for the entire samples to be received over epochs, i.e. the entire snapshot \mathbf{z}_ℓ is needed so that the LMS algorithm can operate. In this context, a purely sequential approximated NLMS is proposed. The advantage of such an implementation is evident, i.e. an estimate of the different AoAs can be achieved per epoch.

Algorithm 2 Sequential NLMS filter

```

INPUT  $\mathbf{Z} = [\mathbf{z}_1 \dots \mathbf{z}_L]$ ,  $\mu$ ,  $\Theta_{\text{grid}}$ 
INIT  $d_\ell(\theta) \leftarrow \mathbf{0}_{N_{\text{grid}} \times L}$ ,  $P(\theta) \leftarrow \mathbf{0}_{N_{\text{grid}} \times 1}$ 
while  $n = 1 \dots N_{\text{epoch}}$  do
     $\hat{\Theta}_{1:K}^{\text{RIS}} = \emptyset$ 
    while  $\theta \neq \emptyset$  do
         $\ell \leftarrow 0$ 
         $p \leftarrow 0$ 
        while  $\ell < L$  do
             $d_\ell(\theta) \leftarrow d_\ell(\theta) + \mathbf{a}^H(\theta) \mathbf{V}_{n,:}^H \mathbf{Z}_{n,\ell}$ 
             $p \leftarrow p + \frac{\mu}{\|\mathbf{z}_{1:n,\ell}\|^2} (d_\ell(\theta) - p^* \mathbf{z}_{n,\ell})^* \mathbf{z}_{n,\ell}$ 
             $\ell \leftarrow \ell + 1$ 
        end while
         $P(\theta) \leftarrow P(\theta) + |p|^2$ 
        Choose next  $\theta \in \Theta_{\text{grid}}$ 
    end while
    if  $P(\theta)$  is peak then
        Insert  $\theta$  in  $\hat{\Theta}_{1:K}^{\text{RIS},(n)}$ 
    end if
end while
return  $\hat{\Theta}_{1:K}^{\text{RIS},(n)}$ 
    
```

It is worth noting that for each epoch n , **Algorithm 2** provides an estimate of the AoAs, i.e. $\hat{\Theta}_{1:K}^{\text{RIS},(n)}$, as opposed to **Algorithm 1**, where we have to wait until the last epoch.

VI. SIMULATION RESULTS

In this section, we present different simulation results, conducted to illustrate the performance of the proposed methods. Furthermore, these methods are compared with a baseline, running the same methods depicted in **Algorithm 1** and **Algorithm 2**, but without an RIS. Unless otherwise stated, we fix the number of epochs used for RIS measurements to $N_{\text{epoch}} = 100$. The number of time samples is set to $L = 100$ samples. Furthermore, the number of antenna elements at the PR is $N_{\text{PR}} = 8$ antennas. The threshold used for peak detection for both batch and sequential NLMS methods described in **Algorithm 1** and **Algorithm 2** is set to $\varphi = 0.5$. Moreover, we fix the angles between the AP and the RIS, and the RIS and the PR to $\theta_{\text{AP}}^{\text{RIS}} = -10^\circ$ and $\theta_{\text{RIS}}^{\text{PR}} = -40^\circ$, respectively. A uniform linear array (ULA) configuration spaced at half a wavelength has been integrated at the PR.

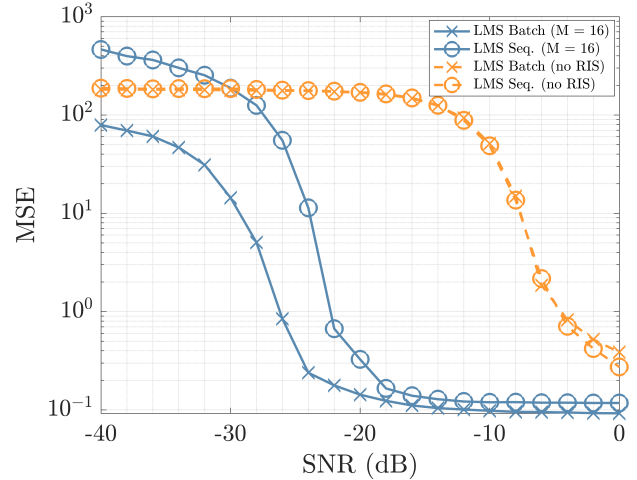


Fig. 2. The MSE vs. SNR performances with $K = 2$ targets, for a ULA configuration of $N_{\text{PR}} = 8$ antennas and $L = 100$ time samples.

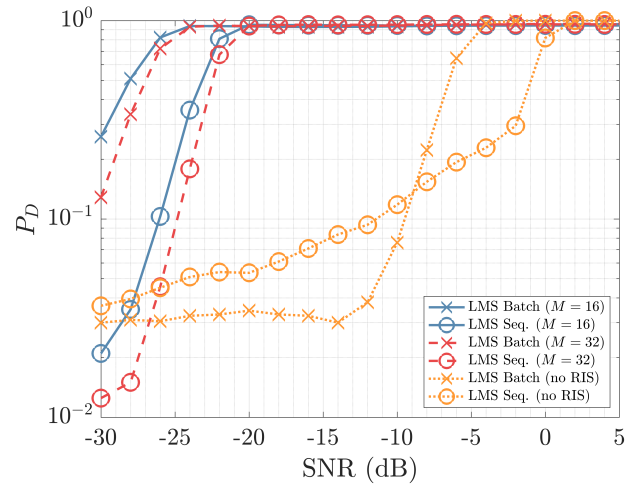


Fig. 3. The probability of detection vs. SNR performances with $N_{\text{PR}} = 8$ antennas and $L = 100$ time samples. Two targets were set in the scene.

In Fig. 2, we aim at analyzing the MSE as a function of SNR at the PR. The MSE is computed as

$$\text{MSE} = \frac{1}{PK} \sum_{k=1}^K \sum_{p=1}^P (\theta_k - \hat{\theta}_k)^2, \quad (35)$$

The SNR at the PR is defined as

$$\text{SNR} = \frac{\mathbb{E} \left(\left| \mathbf{y}_n^{(\text{RIS})}(t) + \mathbf{y}^{(\text{AP})}(t) + \sum_{k=1}^K \mathbf{y}^{(k)}(t) \right|^2 \right)}{\mathbb{E} \left(\left| \boldsymbol{\epsilon}_n(t) \right|^2 \right)}, \quad (36)$$

where

$$\mathbf{y}_n^{(\text{RIS})}(t) = \rho_{\text{RIS}}^{\text{PR}} \mathbf{a}(\theta_{\text{RIS}}^{\text{PR}}) x_n(t - \tau_{\text{RIS}}^{\text{PR}}), \quad (37)$$

$$\mathbf{y}^{(\text{AP})}(t) = \rho_{\text{AP}}^{\text{PR}} \mathbf{a}(\theta_{\text{AP}}^{\text{PR}}) s(t - \tau_{\text{AP}}^{\text{PR}}), \quad (38)$$

$$\mathbf{y}^{(k)}(t) = \rho_k \mathbf{a}(\theta_k^{\text{PR}}) s(t - \tau_{\text{AP}}^k - \tau_k^{\text{PR}}). \quad (39)$$

The parameter θ_k is the true AoA of the k^{th} target and $\hat{\theta}_k$ is the estimated AoA of the k^{th} target. We have simulated two

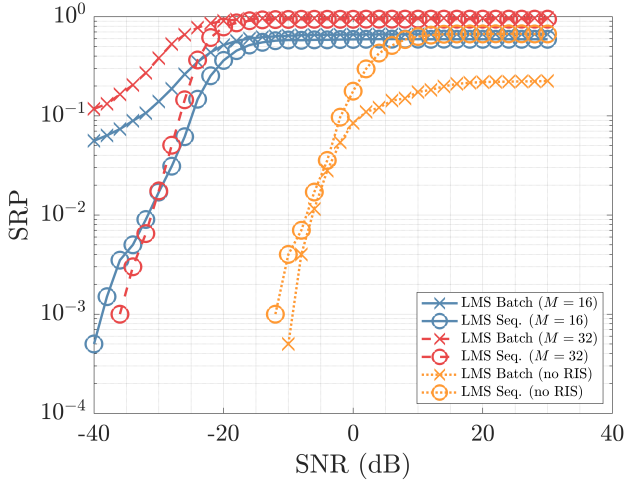


Fig. 4. The SRP vs. SNR performances with $L = 100$ time samples, two targets and $N_{PR} = 8$ antennas.

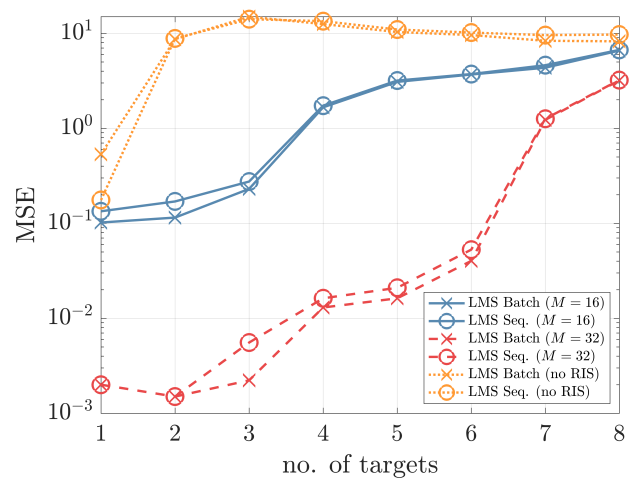


Fig. 6. The MSE behavior against the number of targets K with fixed SNR = 20 dB at the PR.

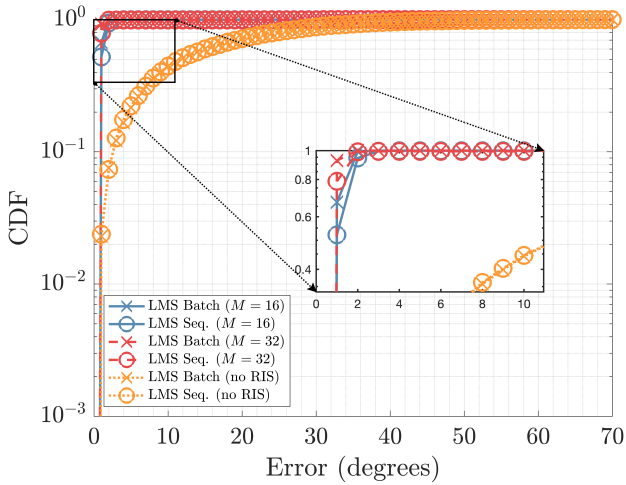


Fig. 5. The CDF performance with $K = 2$ targets, for a ULA configuration of $N_{PR} = 8$ antennas and $L = 100$ time samples.

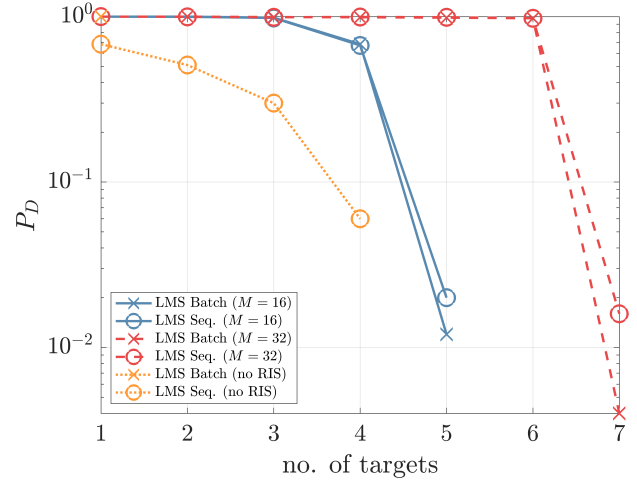


Fig. 7. The detection probability behavior vs. K with fixed SNR = 20 dB at the PR.

targets, i.e. $K = 2$. Also, P is the number of Monte-carlo trials. We observe that at an MSE of 0.2 is achieved with the sequential NLMS method at SNR = -18.55 dB utilizing $M = 16$ reflective elements. The same MSE can be achieved at SNR = -22.8 dB with the batch NLMS method, translating to a gain of 4.25 dB. Comparing both methods to the no-RIS baseline, a gain superior to 20 dB can be attained. This demonstrates the advantage of the proposed RIS-aided model, as the accuracy of the AoA estimates are drastically improved. On the other hand, since the proposed methods also offer joint detection of number of targets, we also study the probability of correct detection for the proposed methods.

In Fig. 3, we study the probability of correct detection of the proposed methods, and compare it with the baseline scheme. The detection probability is computed as follows

$$P_D = \frac{\text{no. of correct target enumeration}}{\text{no. of trials}}. \quad (40)$$

Setting a level of $P_D = 0.9$, and when no RIS is deployed,

the required SNR is SNR = -4.4 dB for batch NLMS, as opposed to SNR = 0.95 dB for sequential NLMS. A gain of 0.95 dB in terms of SNR is noticed, when using an RIS with $M = 16$ reflective elements. An additional 4 dB gain can be attained when doubling the number of RIS reflective elements.

To get a better sense of target localization accuracy, we study the SRP in Fig. 4. To this end, the SRP is defined as follows

$$\text{SRP} = \frac{\text{no. of trials with all } \theta_k = \hat{\theta}_k}{\text{no. of trials}}. \quad (41)$$

As it can be concluded, the non-aided RIS scenario cannot achieve a perfect SRP with $L = 100$ time samples and $N_{PR} = 8$ antenna elements. The SRP is saturated in this case at 66% starting at SNR = 16 dB. In contrast, we observe that 66% SRP can be achieved with SNR = -8 dB with only $M = 16$ reflective elements. Furthermore, and by doubling the number of reflective elements, we can achieve an additional

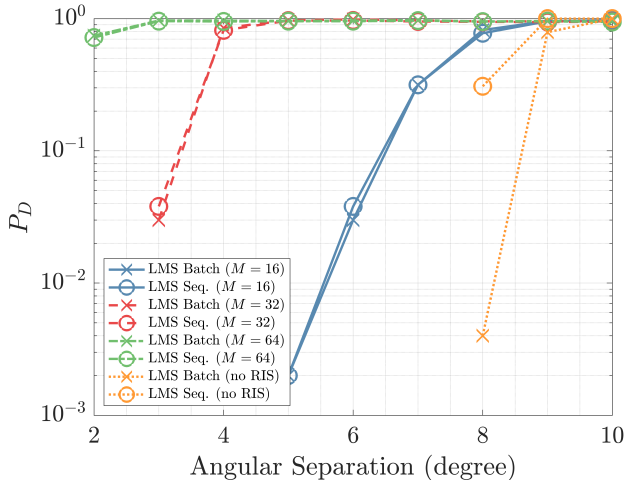


Fig. 8. Detection probability vs. angular separation

gain of about 18 dB, for SRP = 66%. Additionally, the SRP trespasses 95% for $M = 32$ elements when the batch NLMS method is utilized.

Next, we study the CDF as a function of absolute errors in Fig. 5, i.e. $\Pr(|\theta - \hat{\theta}| < e)$. We see that the baseline approach requires an error of $e = 32^\circ$ for a probability of 0.9 for both batch and sequential NLMS algorithms. On the other hand, when adopting the RIS-aided approach, we see that this error can be reduced to an order of magnitude of about 10. Namely, we see that $\Pr(|\theta - \hat{\theta}| < 1.9) = 0.9$ for sequential NLMS and $\Pr(|\theta - \hat{\theta}| < 1.75) = 0.9$ for batch NLMS with $M = 16$ reflective elements. Furthermore, by doubling the number of reflective elements, the error becomes close to the resolution of Θ_{grid} .

Another important performance is the behavior of the MSE, when varying the number of targets in the scene. Each new target introduced in the scene is spaced at 5° further away from the previous target, measured with respect to the RIS. Nevertheless, the SNR at the PR is set to $\text{SNR} = 0$ dB. In Fig. 6, we plot the MSE as a function of number of targets. As we can observe, as soon as we have 2 closely spaced targets, the MSE of both methods trespasses an MSE of 1, when no RIS is employed. However, by using $M = 16$ reflective elements, the number of closely spaced targets that can be resolved with an MSE of 1 almost quadruples. Furthermore, by doubling the number of reflective elements, we can further double the number of targets.

We also study the probability of detection of targets in Fig. 7, for different values of number of targets. The targets are generated the same way as in the previous experiment. Moreover, the SNR at the PR is fixed to $\text{SNR} = 0$ dB. Setting a desired probability of detection to $P_D = 0.9$, we see that a no-RIS approach cannot reach this limit, even with only 1 target. Comparing this baseline scheme with an RIS-aided approach with $M = 16$ reflective elements, we can see that with 3 targets, we are at almost $P_D \simeq 0.98$ for both batch and sequential NLMS methods. We can further double the number of resolvable targets to 6, by doubling the number of reflective

elements at the RIS to $M = 32$.

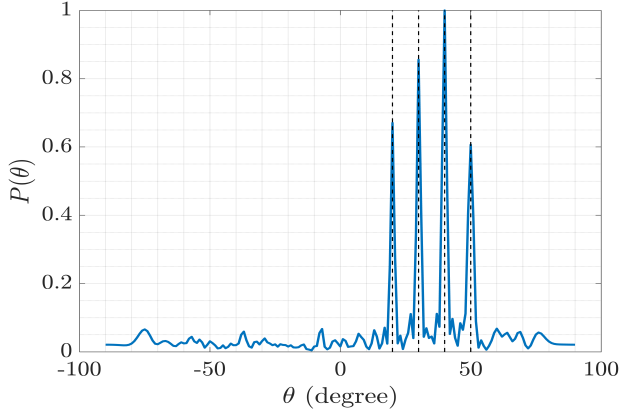
Furthermore, Fig. 8 reports the performance against angular separation. We fix two targets and vary the angle between them, i.e. the second target is placed at $\theta_2 = \theta_1 + \Delta$. Nevertheless, the SNR at the PR is set to 20 dB. In such a setting, results demonstrate that a no-RIS approach requires an angular separation of $\Delta = 9^\circ$ to exceed a level of $P_D = 0.8$. This resolution can be improved by utilizing an RIS-aided scenario with $M = 32$ reflective elements, where for the same P_D , the angular separation is improved by a factor of 2.25, i.e. $\Delta = 4^\circ$. This resolution can even be improved towards $\Delta \simeq 2.3^\circ$ for the same P_D , just by doubling the amount of reflective elements.

Fig. 9 shows the spectra obtained by the proposed NLMS filtering methods, namely Fig. 9a shows the spectrum of **Algorithm 1**, whereas Fig. 9b shows that of **Algorithm 2**. It is clear from both simulations that the peaks are sharp enough to successfully resolve the $K = 4$ targets. Notice that for the sequential NLMS filter, we remind the reader that **Algorithm 2** yields a spectrum $P(\theta)$ per epoch. Naturally, the spectrum starts off with peaks that skew from their true positions, resulting in a poor resolution. Nevertheless, with increasing epoch number, the spectrum smoothes down and peaks converge to their true positions.

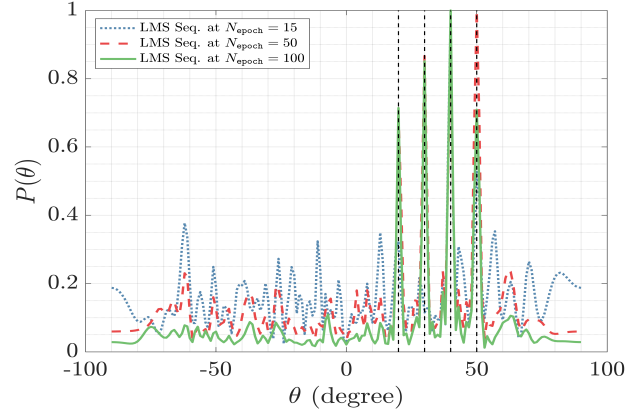
VII. CONCLUSIONS AND FUTURE INSIGHTS

In this manuscript, target localization in terms of AoA is accomplished via a newly proposed architecture well-suited for communication-centric ISAC designs, consisting of an RIS and monitored by a PR, where target detection and estimation are performed. Towards such a setting, we posit an optimization framework enabling us to configure the phase shifters at the RIS in order to reliably mirror the useful reflections caused by the intended targets. Furthermore, we have derived two methods, motivated by the problem of minimal information available at the disposal of the PR. These methods are based on the NLMS filter, and are well-suited for joint detection of number of targets and estimation of the AoAs of the corresponding targets within the proposed RIS-aided communication-centric ISAC architecture. Numerical simulations validate the superior performance of both methods, when applied on the proposed architecture.

Future work will be oriented towards an adaptive beamformer, where the goal would be to learn the covariance matrix of the interference plus noise part, thanks to the target localization part, which could leverage such necessary information for covariance construction. Moreover, further extensions towards more sophisticated infrastructure, such as simultaneous AP transmissions or hybrid RIS where the goal would be to guarantee a reflected signal with good communications and radar characteristics. Furthermore, one could exploit additional sensing parameters with our proposed scenario, such as distance estimation via propagation delays and velocity estimation via doppler information. Also, one could generalize the scenario at hand toward two-dimensional and three-dimensional localization, by exploiting azimuth-elevation information. Even more, multiple RIS could be deployed, therefore, the PR would create multiple beams to align



(a) **Algorithm 1:** NLMS batch method



(b) **Algorithm 2:** NLMS sequential method

Fig. 9. The spectra of the proposed NLMS filtering methods utilizing the RIS-aided architecture. The scene consists of $K = 4$ targets located at $\theta_k^{\text{RIS}} = 20 + 10(k - 1), \forall k$. The RIS is equipped with $M = 64$ reflective elements and the number of time samples is $L = 100$. The number of epochs is set to $N_{\text{epoch}} = 100$. Dashed vertical lines represent the true AoAs.

its look direction at those surfaces. A generalization of the aforementioned direction is to have each RIS oriented towards possibly different objectives, i.e. sensing, communication, and security. Future research will also be shifted towards a deeper analysis oriented towards fundamental limits of the proposed model, i.e. Cramér-Rao bound analysis. This could allow to determine the required number of reflective RIS elements required for a given positioning accuracy.

REFERENCES

- [1] M. Chafii, L. Bariah, S. Muhaidat, and M. Debbah, “Twelve scientific challenges for 6g: Rethinking the foundations of communications theory,” 2022. [Online]. Available: <https://arxiv.org/abs/2207.01843>
- [2] W. Saad, M. Bennis, and M. Chen, “A vision of 6g wireless systems: Applications, trends, technologies, and open research problems,” *IEEE network*, vol. 34, no. 3, pp. 134–142, 2019.
- [3] M. D. Renzo, M. Debbah, D.-T. Phan-Huy, A. Zappone, M.-S. Alouini, C. Yuen, V. Sciancalepore, G. C. Alexandropoulos, J. Hoydis, H. Gacanin *et al.*, “Smart radio environments empowered by reconfigurable ai meta-surfaces: An idea whose time has come,” *EURASIP Journal on Wireless Communications and Networking*, vol. 2019, no. 1, pp. 1–20, 2019.
- [4] Y. Han, S. Jin, C.-K. Wen, and T. Q. Quek, “Localization and channel reconstruction for extra large ris-assisted massive mimo systems,” *IEEE Journal of Selected Topics in Signal Processing*, 2022.
- [5] N. Decarli and D. Dardari, “Communication modes with large intelligent surfaces in the near field,” *IEEE Access*, vol. 9, pp. 165 648–165 666, 2021.
- [6] T. Hou, Y. Liu, Z. Song, X. Sun, Y. Chen, and L. Hanzo, “Mimo assisted networks relying on intelligent reflective surfaces: A stochastic geometry based analysis,” *IEEE Transactions on Vehicular Technology*, vol. 71, no. 1, pp. 571–582, 2021.
- [7] Y. Cheng, K. H. Li, Y. Liu, K. C. Teh, and H. V. Poor, “Downlink and uplink intelligent reflecting surface aided networks: Noma and oma,” *IEEE Transactions on Wireless Communications*, vol. 20, no. 6, pp. 3988–4000, 2021.
- [8] Q. Wu and R. Zhang, “Towards smart and reconfigurable environment: Intelligent reflecting surface aided wireless network,” *IEEE Communications Magazine*, vol. 58, no. 1, pp. 106–112, 2019.
- [9] S. Lin, B. Zheng, G. C. Alexandropoulos, M. Wen, M. Di Renzo, and F. Chen, “Reconfigurable intelligent surfaces with reflection pattern modulation: Beamforming design and performance analysis,” *IEEE transactions on wireless communications*, vol. 20, no. 2, pp. 741–754, 2020.
- [10] X. Pei, H. Yin, L. Tan, L. Cao, Z. Li, K. Wang, K. Zhang, and E. Björnson, “Ris-aided wireless communications: Prototyping, adaptive beamforming, and indoor/outdoor field trials,” *IEEE Transactions on Communications*, vol. 69, no. 12, pp. 8627–8640, 2021.
- [11] W. Xu, J. Zhang, S. Cai, J. Wang, and Y. Wu, “Ris-assisted mimo secure communications with bob’s statistical csi and without eve’s csi,” *Digital Communications and Networks*, 2022.
- [12] G. C. Alexandropoulos, K. Katsanos, M. Wen, and D. B. Da Costa, “Safeguarding mimo communications with reconfigurable metasurfaces and artificial noise,” in *ICC 2021-IEEE International Conference on Communications*. IEEE, 2021, pp. 1–6.
- [13] C. Pradhan, A. Li, L. Song, J. Li, B. Vucetic, and Y. Li, “Reconfigurable intelligent surface (ris)-enhanced two-way ofdm communications,” *IEEE Transactions on Vehicular Technology*, vol. 69, no. 12, pp. 16 270–16 275, 2020.
- [14] S. Lin, B. Zheng, G. C. Alexandropoulos, M. Wen, F. Chen *et al.*, “Adaptive transmission for reconfigurable intelligent surface-assisted ofdm wireless communications,” *IEEE Journal on Selected Areas in Communications*, vol. 38, no. 11, pp. 2653–2665, 2020.
- [15] G. Zhou, C. Pan, H. Ren, P. Popovski, and A. L. Swindlehurst, “Channel estimation for ris-aided multiuser millimeter-wave systems,” *IEEE Transactions on Signal Processing*, vol. 70, pp. 1478–1492, 2022.
- [16] K. Ardah, S. Gherekhloo, A. L. de Almeida, and M. Haardt, “Trice: A channel estimation framework for ris-aided millimeter-wave mimo systems,” *IEEE signal processing letters*, vol. 28, pp. 513–517, 2021.
- [17] H. Liu, J. Zhang, Q. Wu, H. Xiao, and B. Ai, “Admm based channel estimation for riss aided millimeter wave communications,” *IEEE communications letters*, vol. 25, no. 9, pp. 2894–2898, 2021.
- [18] J. He, H. Wymeersch, and M. Juntti, “Channel estimation for ris-aided mmwave mimo systems via atomic norm minimization,” *IEEE Transactions on Wireless Communications*, vol. 20, no. 9, pp. 5786–5797, 2021.
- [19] Y. Liu, X. Liu, X. Mu, T. Hou, J. Xu, M. Di Renzo, and N. Al-Dhahir, “Reconfigurable intelligent surfaces: Principles and opportunities,” *IEEE Communications Surveys & Tutorials*, vol. 23, no. 3, pp. 1546–1577, 2021.
- [20] C. Huang, A. Zappone, G. C. Alexandropoulos, M. Debbah, and C. Yuen, “Reconfigurable intelligent surfaces for energy efficiency in wireless communication,” *IEEE Transactions on Wireless Communications*, vol. 18, no. 8, pp. 4157–4170, 2019.
- [21] C. Huang, G. C. Alexandropoulos, A. Zappone, M. Debbah, and C. Yuen, “Energy efficient multi-user miso communication using low resolution large intelligent surfaces,” in *2018 IEEE Globecom Workshops (GC Wkshps)*. IEEE, 2018, pp. 1–6.
- [22] S. Zhou, W. Xu, K. Wang, M. Di Renzo, and M.-S. Alouini, “Spectral and energy efficiency of irs-assisted miso communication with hardware impairments,” *IEEE Wireless Communications Letters*, vol. 9, no. 9, pp. 1366–1369, 2020.
- [23] M. Cui, G. Zhang, and R. Zhang, “Secure wireless communication via

- intelligent reflecting surface,” *IEEE Wireless Communications Letters*, vol. 8, no. 5, pp. 1410–1414, 2019.
- [24] C. Liaskos, A. Tsioliaridou, A. Pitsillides, S. Ioannidis, and I. Akyildiz, “Using any surface to realize a new paradigm for wireless communications,” *Communications of the ACM*, vol. 61, no. 11, pp. 30–33, 2018.
- [25] B. Dawidowicz, P. Samczynski, M. Malanowski, J. Misiurewicz, and K. Kulpa, “Detection of moving targets with multichannel airborne passive radar,” *IEEE Aerospace and Electronic Systems Magazine*, vol. 27, no. 11, pp. 42–49, 2012.
- [26] E. Finden, J. M. Christiansen, Ø. Lie-Svendsen, and K. E. Olsen, “Analysis of detection performance of incoherent range walk compensation for passive radar,” in *2015 16th International Radar Symposium (IRS)*. IEEE, 2015, pp. 30–35.
- [27] P. Krysiak, M. Wielgo, J. Misiurewicz, and A. Kurowska, “Doppler-only tracking in gsm-based passive radar,” in *17th International Conference on Information Fusion (FUSION)*. IEEE, 2014, pp. 1–7.
- [28] J. E. Palmer, H. A. Harms, S. J. Searle, and L. Davis, “Dvb-t passive radar signal processing,” *IEEE transactions on Signal Processing*, vol. 61, no. 8, pp. 2116–2126, 2012.
- [29] E. C. Strinati, G. C. Alexandropoulos, V. Sciancalepore, M. Di Renzo, H. Wymeersch, D.-T. Phan-Huy, M. Crozzoli, R. d’Errico, E. De Carvalho, P. Popovski *et al.*, “Wireless environment as a service enabled by reconfigurable intelligent surfaces: The rise-6g perspective,” in *2021 Joint European Conference on Networks and Communications & 6G Summit (EuCNC/6G Summit)*. IEEE, 2021, pp. 562–567.
- [30] H. Kuschel, D. Cristallini, and K. E. Olsen, “Tutorial: Passive radar tutorial,” *IEEE Aerospace and Electronic Systems Magazine*, vol. 34, no. 2, pp. 2–19, 2019.
- [31] A. Bazzi and M. Chafii, “On outage-based beamforming design for dual-functional radar-communication 6g systems,” *arXiv preprint arXiv:2207.04921*, 2022.
- [32] D. Xu, X. Yu, D. W. K. Ng, A. Schmeink, and R. Schober, “Robust and secure resource allocation for isac systems: A novel optimization framework for variable-length snapshots,” *arXiv preprint arXiv:2206.13307*, 2022.
- [33] A. W. Azim, A. Bazzi, R. Shubair, and M. Chafii, “Dual-mode chirp spread spectrum modulation,” *IEEE Wireless Communications Letters*, vol. 11, no. 9, pp. 1995–1999, 2022.
- [34] A. Taha, M. Alrabeiah, and A. Alkhateeb, “Enabling large intelligent surfaces with compressive sensing and deep learning,” *IEEE access*, vol. 9, pp. 44 304–44 321, 2021.
- [35] J. He, H. Wymeersch, T. Sanguanpuak, O. Silvén, and M. Juntti, “Adaptive beamforming design for mmwave ris-aided joint localization and communication,” in *2020 IEEE Wireless Communications and Networking Conference Workshops (WCNCW)*. IEEE, 2020, pp. 1–6.
- [36] A. Fascista, A. Coluccia, H. Wymeersch, and G. Seco-Granados, “Ris-aided joint localization and synchronization with a single-antenna mmwave receiver,” in *ICASSP 2021-2021 IEEE International Conference on Acoustics, Speech and Signal Processing (ICASSP)*. IEEE, 2021, pp. 4455–4459.
- [37] A. Elzanaty, A. Guerra, F. Guidi, and M.-S. Alouini, “Reconfigurable intelligent surfaces for localization: Position and orientation error bounds,” *IEEE Transactions on Signal Processing*, vol. 69, pp. 5386–5402, 2021.
- [38] H. Zhang, H. Zhang, B. Di, K. Bian, Z. Han, and L. Song, “Metalocalization: Reconfigurable intelligent surface aided multi-user wireless indoor localization,” *IEEE Transactions on Wireless Communications*, vol. 20, no. 12, pp. 7743–7757, 2021.
- [39] —, “Towards ubiquitous positioning by leveraging reconfigurable intelligent surface,” *IEEE Communications Letters*, vol. 25, no. 1, pp. 284–288, 2020.
- [40] H. Akaike, “Information theory and an extension of the maximum likelihood principle,” in *Selected papers of hirotugu akaike*. Springer, 1998, pp. 199–213.
- [41] J. Rissanen, “Modeling by shortest data description,” *Automatica*, vol. 14, no. 5, pp. 465–471, 1978.
- [42] S. Haykin, “Adaptive filter theory 3rd edition prentice-hall,” 1996.